

BIOCHEMISTRY

Promotion of row 1–specific tip complex condensates by Gpsm2-Gai provides insights into row identity of the tallest stereocilia

Yingdong Shi^{1†}, Lin Lin^{2†}, Chao Wang^{1*}, Jinwei Zhu^{2*}

The mechanosensory stereocilia in hair cells are organized into rows of graded height, a property crucial for auditory perception. Gpsm2-Gai-Whirlin-Myo15-Eps8 complex at tips of the tallest stereocilia is proposed to define hair bundle row identity, although the underlying mechanism remains elusive. Here, we find that Gpsm2 could undergo phase separation. Moreover, row 1–specific Gpsm2-Gai complex significantly promotes the formation of the five-component tip complex density (5xTCD) condensates. The 5xTCD condensates display much stronger actin-bundling ability than those without Gpsm2-Gai, which may provide critical insights into how Gpsm2-Gai specifies the tallest stereocilia. A deafness-associated mutation of Gpsm2 leads to impaired formation of the 5xTCD condensates and consequently reduced actin bundling, providing possible clues for etiology of hearing loss in patients with Chudley-McCullough syndrome.

INTRODUCTION

Sound detection relies on the epithelial mechanosensory hair cells in the cochlea of inner ear. The mechanically sensitive organelles of hair cells are stereocilia, a cluster of actin-rich protrusions at their apical surface (1, 2). Stereocilia are interconnected by several kinds of hair bundle links such as tip links (3, 4). A unique structural feature of stereocilia is that they are organized into rows of graded height (5) (Fig. 1A). Such a staircase-like pattern is critical for mechanosensory transduction. Mechanical force evoked by sound waves results in stereocilia deflection toward the tallest row, which, in turn, activates the mechano-electrical transducer channels located in the shorter stereocilia, thus achieving the mechano-electrical transduction (1, 6).

Proper development of stereocilia is essential for auditory perception, as manifested by severe hearing loss caused by genetic mutations of genes that regulate stereocilia growth (2, 4). Many of these genes encode actin cytoskeleton regulatory proteins that locate at the electron-dense areas of the distal tips of stereocilia (7, 8), playing crucial roles in promoting actin polymerization and bundling. Examples are Whirlin, myosin 15 (Myo15), and epidermal growth factor receptor pathway substrate 8 (Eps8) (9–11). Mice deficient in any of these three genes exhibited similar stereocilia stunting and profound deafness (10, 12, 13). Mechanistically, we and others demonstrated that the three proteins can directly interact with one another to form a tight complex (14, 15) (Fig. 1B). These interactions allow Myo15 motor to transport protein cargos (Whirlin and Eps8) within developing stereocilia where Eps8, an evolutionarily conserved cytoskeletal effector, executes its actin-capping and actin-bundling activities (9). Moreover, the ternary complex forms liquid-liquid

phase separation (LLPS) in vitro and in living cells and facilitates actin bundling, indicating that the electron-dense areas located at the tips of stereocilia may form via LLPS of the tip complex in all rows (14).

However, it still remains unclear how stereocilia adopt such a staircase-like architecture and what determines the row identity of the tallest stereocilia. Given the planar asymmetry in the staircase pattern of stereocilia, recent studies on planar cell polarity may provide crucial clues for the possible underlying mechanism (16–20). A complex of Inscuteable (Insc), G protein signaling modulator 2 (Gpsm2; also known as LGN), and heterotrimeric G protein Gai (i.e., mInsc-Gpsm2-Gai complex) defines an apical compartment (termed as the “bare zone”) with a sharp microvilli exclusion boundary along the mediolateral planar polarity axis to create the V-shaped hair bundles (16). Most notably, Gpsm2-Gai is then restrictedly enriched at the distal tips of stereocilia abutting the bare zone that later become the tallest row (row 1), colocalized with Whirlin, Myo15, and Eps8 (18, 21) (Fig. 1A). Mice deficient in *Gpsm2* or *Gnai* (encoding Gai) showed similar stereocilia stunting and severe hearing loss as *whirler* mice (inactivating Whirlin), *shaker-2* mice (lacking Myo15), and *Eps8*-knockout mice did (18, 22–24). Recently, mutations in *Gpsm2* were found in patients with Chudley-McCullough syndrome (CMCS; Online Mendelian Inheritance in Man: 604213), a rare autosomal recessive disease characterized by severe to profound sensorineural hearing loss and partial agenesis of the corpus callosum (25–27). Moreover, Gpsm2 was found to interact with Whirlin directly, colocalized into a highly dense nanodomain with a cap-like structure at the tips of the tallest stereocilia (23). Therefore, the five components (Myo15, Eps8, Whirlin, Gpsm2, and Gai) at the tips of the tallest stereocilia may operate in the same pathway to determine the row identity, although the underlying mechanism is largely unclear.

In this study, we characterize the Gpsm2-Whirlin interaction in detail through a combination of biochemical and biophysical approaches. We found that Gpsm2 itself could form LLPS in vitro and in cells. Gpsm2-Gai significantly promotes the formation of the five-component tip complex density (5xTCD) condensates (Gpsm2-Gai-Whirlin-Myo15-Eps8). The promotion effect is most likely due to Gpsm2 LLPS, as a mutant of Gpsm2 that disrupts its LLPS largely impairs the 5xTCD condensates formation. Consistent with their

¹Department of Neurology, the First Affiliated Hospital of USTC, Ministry of Education Key Laboratory for Cellular Dynamics, Biomedical Sciences and Health Laboratory of Anhui Province, School of Life Sciences, Division of Life Sciences and Medicine, University of Science and Technology of China, Hefei 230027, China. ²Bio-X Institutes, Key Laboratory for the Genetics of Developmental and Neuropsychiatric Disorders, Ministry of Education, Shanghai Jiao Tong University, Shanghai 200240, China.

*Corresponding author. Email: cwangust@ustc.edu.cn (C.W.); jinwei.zhu@sjtu.edu.cn (J.Z.)

†These authors contributed equally to this work.

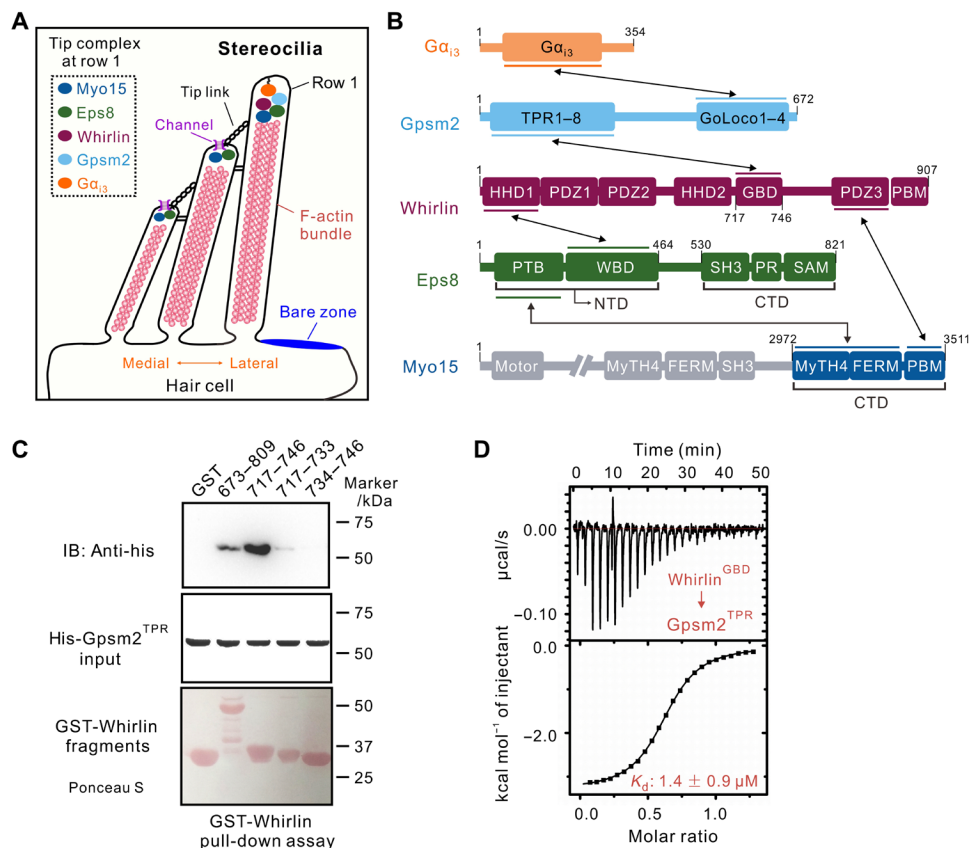


Fig. 1. The Gpsm2-Whirlin interaction. (A) A schematic diagram illustrating the organization of hair cell stereocilia. An apical compartment (termed as the “bare zone”) with a sharp microvilli exclusion boundary along the mediolateral planar polarity axis is highlighted with a blue area. The five-component tip complex is also shown. (B) Domain organizations of key components of the tip complex in stereocilia. The two-way arrows indicate direct interactions. TPR, tetratricopeptide repeat; HHD, harmonin homology domain; PDZ, PSD-95/Discs-large/ZO-1 homology; PBM, PDZ binding domain; PTB, phosphotyrosine binding; WBD, Whirlin binding domain; SH3, src homology 3; PR, proline-rich region; SAM, sterile alpha motif; MyTH4, myosin tail homology 4; FERM, 4.1/ezrin/radixin/moesin; GBD, Gpsm2-binding domain; NTD, N-terminal domain; CTD, C-terminal domain. Note that Eps8^{NTD} contains PTB and WBD domains; Eps8^{CTD} contains SH3, PR, and SAM domains with actin-bundling activity. Myo15^{CTD} contains C-terminal MyTH4, FERM, and PBM domains, amino acids 2972 to 3511. Myo15^{CTD} was used in the in vitro condensate reconstitution assays. (C) GST pull-down assays showing that the minimal GBD on Whirlin is the fragment encompassing amino acids 717 to 746. Gpsm2^{TPR}: amino acids 15 to 350; IB, immunoblot. (D) ITC assay showing the binding affinity between Gpsm2^{TPR} and Whirlin^{GBD}.

LLPS capabilities, 5xTCD condensates display much stronger actin-bundling ability than Myo15-Eps8 and Whirlin-Myo15-Eps8 do, which may provide critical insights into how Gpsm2-Gα₃ specifies the tallest stereocilia and defines hair bundle row identity. Notably, a CMCS-associated mutation of Gpsm2 interferes with the condensate formation and consequently impairs actin bundling, offering possible clues for the etiology of CMCS-related hearing loss.

RESULTS

Characterization of the Gpsm2-Whirlin interaction

Gpsm2-Gα₃ requires Whirlin as an adaptor to reach the tips of the tallest stereocilia and form the Myo15-Eps8-Whirlin-Gpsm2-Gα₃ complex specific to row 1 (21). We first set to dissect the interaction between Gpsm2 and Whirlin. Previous report showed that a fragment of Whirlin [amino acids 672 to 810] interacted with N-terminal domain of Gpsm2 (23). Gpsm2 contains eight tetratricopeptide repeats (TPRs) at its N terminus [hereafter Gpsm2^{TPR} (amino acids 15 to 350)] and four GoLoco (GL) motifs at its C terminus (Fig. 1B). During mitotic spindle orientation of asymmetric cell division, Gpsm2 serves

as an adaptor linking the spindle orientation machinery with the cortical polarity cue(s) by binding to mInsc and the nuclear mitotic apparatus (NuMA) via its TPRs and Gα₃ via its GLs, respectively (28). We confirmed the Gpsm2-Whirlin interaction by showing that glutathione *S*-transferase (GST)-Whirlin⁶⁷³⁻⁸⁰⁹ effectively bound to purified Gpsm2^{TPR} (Fig. 1C). Further truncation-based binding assays indicated that Whirlin⁷¹⁷⁻⁷⁴⁶ (hereafter Whirlin^{GBD}, short for Gpsm2-binding domain) was sufficient and necessary for Gpsm2^{TPR} binding, as further deletion of Whirlin^{GBD} either at its N terminus (Whirlin⁷³⁷⁻⁷⁴⁶) or C terminus (Whirlin⁷¹⁷⁻⁷³³) diminished the binding (Fig. 1C). Moreover, isothermal titration calorimetry (ITC)-based assay using highly purified proteins showed that Gpsm2^{TPR} binds to Whirlin^{GBD} with a dissociation constant (K_d) of ~1.4 μM (Fig. 1D).

Gpsm2-Whirlin complex structure

To gain insights into the assembly principles of the Gpsm2-Whirlin complex, we tried to crystallize a chimeric construct in which Whirlin^{GBD} was fused C-terminally to Gpsm2^{TPR}. We were able to obtain crystals of the chimera diffracting to 2.6-Å resolution. We solved the complex structure by molecular replacement and refined

it to an R_{free} of 28.3 and an R_{work} of 23.1 (table S1). The final structure includes the entire length of Gpsm2^{TPR} and amino acids 729 to 743 of Whirlin.

In the complex structure, Gpsm2^{TPR} folds as a right-handed superhelix creating an inner concave groove that holds the extended Whirlin^{GBD} peptide in an antiparallel manner (Fig. 2, A and B). Each TPR repeat consists of two helices, α A and α B, connected by a short loop (Fig. 2A). The eight TPRs pack together to form a curved α -helical solenoid, with α A helices facing the inner surface contacting the elongated Whirlin^{GBD} peptide (Fig. 2A). It is noted that the overall conformation of the assembly is reminiscent of those of Gpsm2^{TPR} in complex with other partners such as NuMA, Insc, and Afadin (fig. S1) (29–32).

The Gpsm2-Whirlin interface

The Gpsm2^{TPR}-Whirlin^{GBD} interface is mainly mediated by electrostatic interactions and hydrogen bonding interactions. R221/R236 and K106 from Gpsm2^{TPR} form salt bridges with E732^{Whirlin} and D734^{Whirlin}, respectively (Fig. 2C). The side chain of Y139^{Gpsm2}

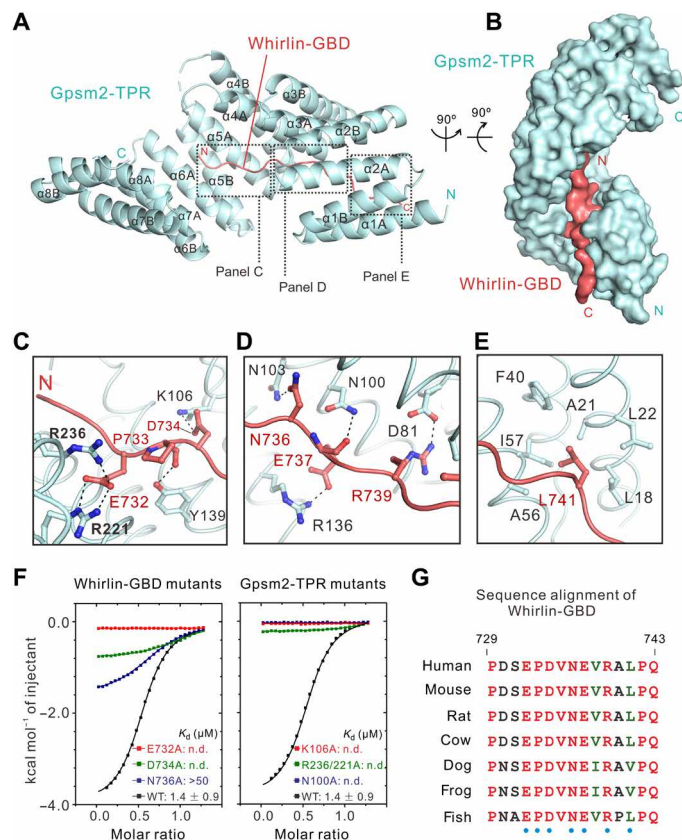


Fig. 2. Crystal structure of Gpsm2-Whirlin complex. (A and B) Ribbon (A) and surface (B) diagram representation of the Gpsm2^{TPR}-Whirlin^{GBD} complex structure. (C to E) Detailed interfaces between Gpsm2^{TPR} and Whirlin^{GBD}. Residues involved in the interaction are shown with the stick model. Hydrogen bonds are shown as black dashed lines. (F) Summary of ITC-based measurements of binding affinities between wild type or mutants of Gpsm2^{TPR} and Whirlin^{GBD}. n.d., not detectable. (G) Sequence alignment of the Whirlin fragment (amino acids 729 to 743) observed in the complex structure from different species. In this alignment, the absolutely conserved and conserved residues are colored in red and green, respectively. Residues involved in binding to Gpsm2^{TPR} are annotated below as blue dots.

forms a hydrogen bond with the main chain of P733^{Whirlin} (Fig. 2C). N100^{Gpsm2} and R136^{Gpsm2} form a hydrogen bond and a salt bridge with the main chain and side chain of E737^{Whirlin}, respectively (Fig. 2D). D81^{Gpsm2} forms additional electrostatic interaction with R739^{Whirlin} (Fig. 2D). It should be mentioned that the hydrophobic interaction between L741^{Whirlin} and L18/A21/L22/F40/A56/I57 from Gpsm2^{TPR} further stabilizes the complex assembly (Fig. 2E). Consistently, mutations that disrupt these polar interactions weakened or even abolished the Gpsm2^{TPR}-Whirlin^{GBD} interaction in ITC-based assays (Fig. 2F). In particular, substitution of E732 of Whirlin^{GBD} with Ala totally abolished the interaction (Fig. 2F), suggesting that E732 is essential for the interaction, which explains why Whirlin⁷³⁴⁻⁷⁴⁶ did not interact with Gpsm2^{TPR} in the GST pull-down assay (Fig. 1C). Notably, key residues in Whirlin^{GBD} that contribute to the interface are absolutely conserved among different species (Fig. 2G), implying the indispensable function of the Gpsm2-Whirlin complex throughout the evolution.

Gpsm2 undergoes phase separation in vitro and in living cells

During our investigation of the Gpsm2-Whirlin interaction in cells, we found an interesting discovery that red fluorescent protein (RFP)-Gpsm2 formed condensed puncta in the cytoplasm when expressed in cells (Fig. 3A). In a fluorescence recovery after photobleaching (FRAP) experiment, RFP signals rapidly recovered after photobleaching over a short period of time (Fig. 3, A and B), indicating that RFP-Gpsm2 could freely exchange between the puncta and the surrounding cytoplasm. We next purified full-length Gpsm2 protein and found that it became turbid at room temperature and turned clear after cooling on ice. The turbid solution formed many spherical liquid-like droplets under differential interference contrast (DIC) microscopy (Fig. 3C). Furthermore, Cy3-labeled Gpsm2 formed spherical droplets in a concentration-dependent manner under fluorescence microscopy (Fig. 3C). These droplets could fuse with each other over time (Fig. 3D). Quantification of distribution of droplet sizes both in cells and in vitro revealed that the diameter of most droplets was within the range of 1 to 3 μm (fig. S2). The aforementioned biophysical features of Gpsm2 are reminiscent of biomolecular condensates formed via LLPS in many systems, suggesting that Gpsm2 can autonomously undergo LLPS in vitro and in living cells. Notably, the number of Gpsm2 droplets decreased when the salt concentration was elevated (Fig. 3E), indicating that electrostatic interaction may contribute to LLPS of Gpsm2.

To figure out the mechanism of phase separation of Gpsm2, we made a variety of truncation and deletion of Gpsm2 and investigated their LLPS abilities (Fig. 3F). Deletion of either TPR domain (TPR1 to TPR8) or GL motifs significantly disrupted LLPS (Fig. 3G). Deletion of a linker region (amino acids 421 to 476) between TPR and GL domains also disrupted LLPS. A unique characteristic of this linker is its enrichment with lysine residue (Lys, K) (this linker is hereafter named as “poly-K loop”) (Fig. 3F and fig. S3). We replaced all the lysine residues with Ala (referred to as the “KA” mutant) and found that the Gpsm2^{KA} mutant failed to form LLPS (Fig. 3G). These results, together with the fact that LLPS of Gpsm2 is highly sensitive to salt concentration, indicated that Gpsm2 LLPS may form via multivalent electrostatic interactions between the poly-K loop and other negative charged surface(s) of Gpsm2. Intriguingly, careful sequence analysis revealed that the poly-K loop is absent in activator of G protein signaling 3 (AGS3; also known as Gpsm1), a close

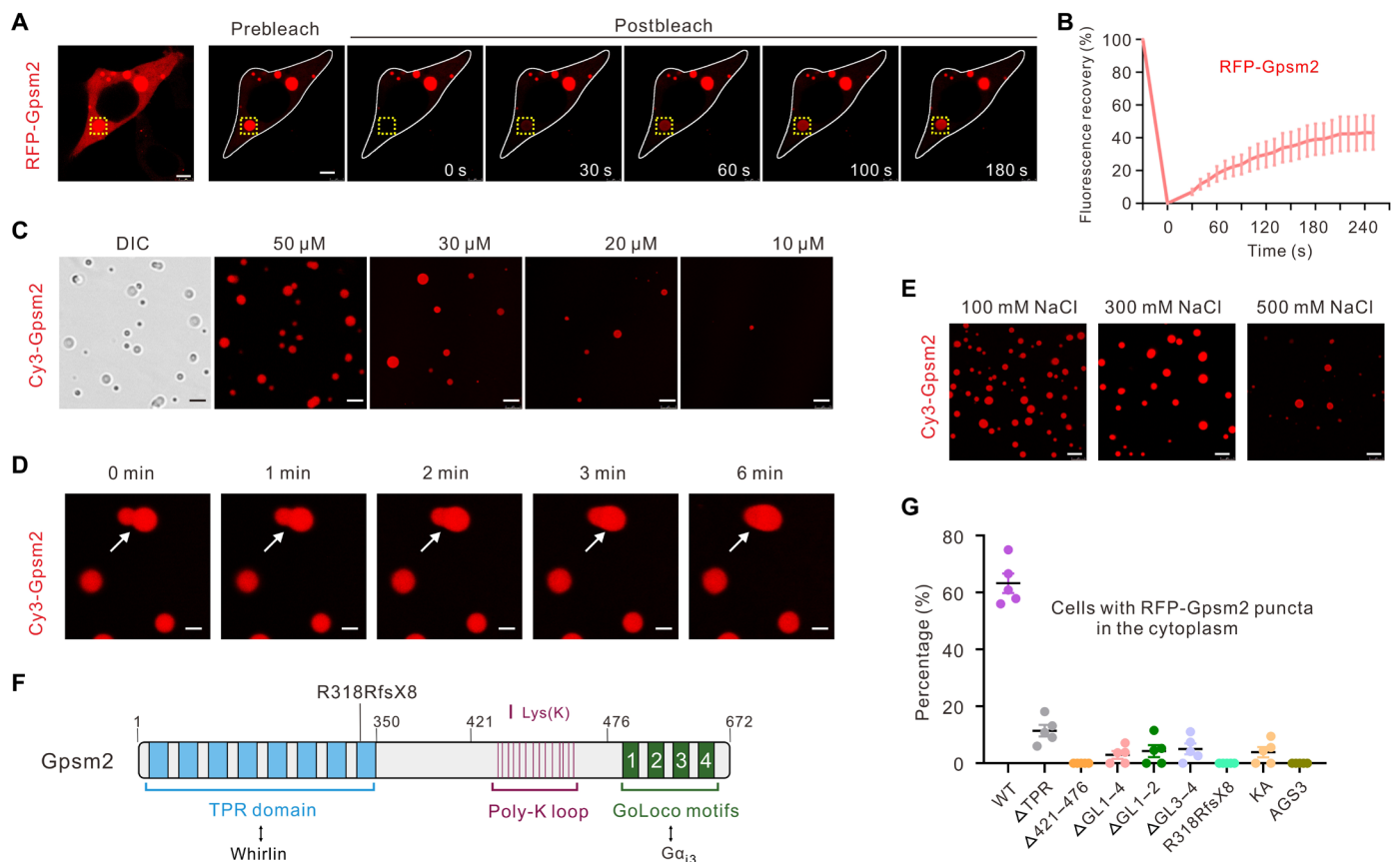


Fig. 3. Gpsm2 undergoes phase separation in vitro and in living cells. (A) Representative images showing expression of RFP-Gpsm2 in human embryonic kidney (HEK) 293T cells produced many spherical puncta. FRAP experiments showing that RFP-Gpsm2 signals recovered quickly after photobleaching within a short period of time. The photobleached area is indicated with a yellow dotted box. Scale bar, 5 μ m. (B) Quantitative results for FRAP experiments of RFP-Gpsm2 in puncta and cytoplasm of HEK293T cells. Time 0 refers to the time point of the photobleaching pulse. All data are represented as means \pm SEM from five droplets ($n = 5$) in cells. (C) Representative DIC and fluorescence images showing that purified full-length Gpsm2 protein underwent phase separation at indicated concentrations. Gpsm2 was sparsely labeled by Cy3 at 1%. Scale bar, 5 μ m. (D) Representative images showing the Gpsm2 liquid-like droplets (indicated by arrows) fused with each other over time. Scale bar, 1 μ m. (E) Fluorescence images showing that the number of the Gpsm2 droplets were reduced with increased NaCl concentration. Scale bar, 5 μ m. (F) Schematic diagram showing the domain organization of Gpsm2. The deafness-associated mutation Gpsm2^{R318RfsX8} was also indicated. Note that there is a lysine-rich region (poly-K loop) in the linker region between TPR and GL domains. (G) The percentage of cells showing spherical puncta with various Gpsm2 constructs. All data are expressed as means \pm SEM. Five batches of cultures with 30 cells counted in each batch.

homolog of Gpsm2, although the two proteins share highly conserved functional domains (fig. S3). Given the essential role of the poly-K loop in LLPS, AGS3, which lacks this sequence, did not form LLPS as expected (Fig. 3G).

A CMCS-associated mutation interferes with Gpsm2 LLPS

Notably, a mutation of *Gpsm2*, p.R318RfsX8, was found in patients with CMCS (23). p.R318RfsX8 encodes a truncated protein lacking the poly-K loop and all four GL motifs (Fig. 3F). Because key elements required for LLPS are missing in this truncated protein, Gpsm2^{R318RfsX8} failed to form LLPS as expected (Fig. 3G).

Cocondensation of Gpsm2 and Whirlin

We recently showed that Whirlin could form phase-separated condensation both in vitro and in living cells (14). Because Gpsm2 physically interacts with Whirlin, we next wondered whether the Gpsm2 condensates and the Whirlin condensates can coexist with each other. Green fluorescent protein (GFP)-Whirlin perfectly colocalized with

RFP-Gpsm2 in the bright puncta when they were coexpressed in human embryonic kidney (HEK) 293T cells (Fig. 4A). Both GFP and RFP signals in the puncta could recover after photobleaching within a short period of time (Fig. 4B). We also found that mixing equal amounts of Cy5-labeled Gpsm2 and Cy3-labeled Whirlin gave rise to condensed liquid-like codroplets in solution (Fig. 4C). FRAP assay showed that both proteins could exchange between the condensed phase and the aqueous solution, although the recovery rates were slower than those in cells (Fig. 4D). Collectively, these results indicated that Gpsm2 and Whirlin could form cocondensates both in vitro and in cells.

Reconstitution of 5xTCD condensates

Myo15, Eps8, Whirlin, Gpsm2, and Gai interact with each other to form a five-component tip complex specific to the tallest stereocilia (Fig. 1B). Thus, we reasonably hypothesized that Myo15, Eps8, and Gai could be recruited to the Gpsm2-Whirlin cocondensates because of the interaction network. We tried to verify this point by

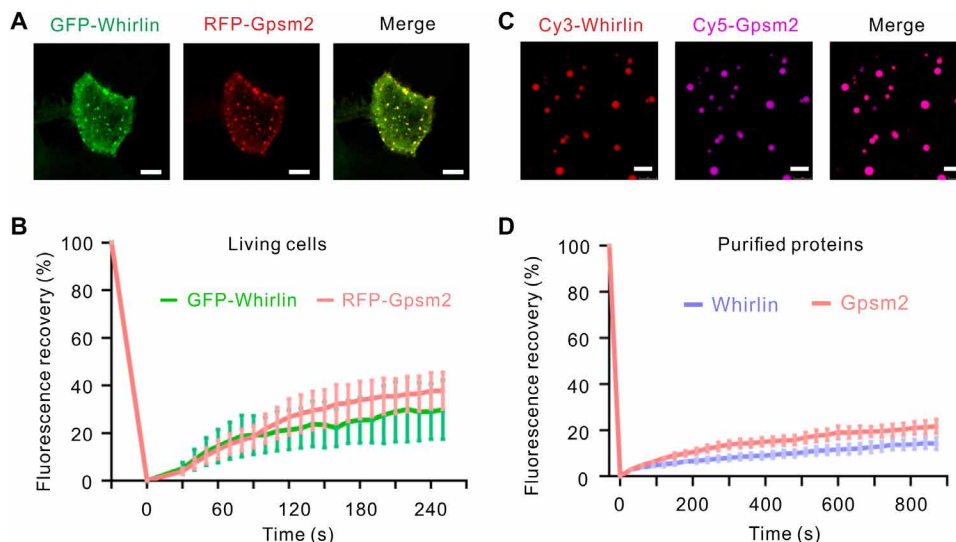


Fig. 4. Cocondensation of Gpsm2 and Whirlin. (A) Representative images showing coexpression of GFP-Whirlin and RFP-Gpsm2 in HEK293T cells produced many spherical puncta with both proteins colocalized with each other. Scale bar, 5 μm . (B) FRAP experiment showing the exchange kinetics of each protein between the condensed puncta and dilute cytoplasm. All data are represented as means \pm SEM from five droplets ($n=5$) in cells. (C) Representative fluorescence images showing that mixture of purified Whirlin and Gpsm2 protein at their individual concentration of 10 μM led to formation of the liquid-like droplets. Whirlin and Gpsm2 were labeled with Cy3 and Cy5, respectively, with each at 1% level. Scale bar, 5 μm . (D) FRAP experiments showing the exchange kinetics of each protein between the condensates and dilute solution. All data are represented as means \pm SEM from five independent experiments ($N=5$).

reconstitution of the five-component complex *in vitro*. We were able to purify all these proteins except full-length Myo15 (14). Instead, we successfully purified a truncated form of Myo15 (i.e., C-terminal myosin tail homology 4–4.1/ezrin/radixin/moesin–PDZ binding motif, amino acids 2972 to 3511) that includes both binding sites for Whirlin and Eps8 (Fig. 1B) (14). In the following reconstitution assays, we refer this truncated protein as Myo15^{CTD}. Notably, although we were able to purify full-length Eps8 (Eps8^{FL}), however, the amount of Eps8^{FL} was relatively limited, which is not suitable for extensive phase separation study. Instead, we were able to obtain a large amount of a truncated Eps8 (Eps8^{NTD}; Fig. 1B) which includes the both binding sites for Whirlin and Myo15. Notably, Eps8^{NTD} and Eps8^{FL} showed comparable effect on assembly of TCD condensates (fig. S4). Therefore, we used Eps8^{NTD} in the following *in vitro* reconstitution assay, which was in accordance with our previous work (14). All the protein used in the reconstitution assays were freshly purified and behaved well (fig. S5).

We intended to study LLPS of the five-component complex using labeled proteins under fluorescence microscopy. However, because of the limitation of the fluorescence microscopy technology, we were only able to simultaneously label four proteins at a time. Therefore, we decided to stain for different combinations of the five components. First, we chose not to label Myo15^{CTD} for it could be recruited to the Whirlin condensates together with Eps8^{NTD} in our previous study (14). When mixing fluorescently labeled Eps8^{NTD} (Alexa Fluor 488), Whirlin (Cy3), Gpsm2 (Cy5), and G α_{13} (Alexa Fluor 405) at a 1:1:1:1 molar ratio at their individual concentration of 5 μM , we readily observed micrometer-sized, liquid-phase droplets with spherical shapes under fluorescence microscopy (Fig. 5A). Then, we chose not to label Whirlin and found that Eps8^{NTD} (Alexa Fluor 488), Myo15^{CTD} (Cy3), Gpsm2 (Cy5), and G α_{13} (Alexa Fluor 405) formed droplets as well (Fig. 5A). Fluorescence images showed that each droplet was highly enriched with each component of the tip complex (Fig. 5A).

These data strongly indicated that the five-component complex can form liquid-phase condensation. To further verify this point, we treated the 5xTCD condensates with 1,6-hexanediol, which has been widely used for LLPS study. Treatment of 1,6-hexanediol greatly impaired the LLPS (Fig. 5B), indicating the reversible character of the 5xTCD condensates. Formation of five-component tip complex condensates was highly specific as they cannot form droplets with an unrelated protein, thioredoxin (Trx) (fig. S6).

Gpsm2-Gai significantly promotes LLPS of Whirlin-Myo15^{CTD}-Eps8^{NTD} condensates

Because both Whirlin-Myo15^{CTD}-Eps8^{NTD} (3xTCD) condensates and 5xTCD condensates formed via LLPS, we intended to systematically compare the phase separation abilities among 3xTCD, 4xTCD^{Gpsm2} (Gpsm2-Whirlin-Myo15^{CTD}-Eps8^{NTD}), 4xTCD^{Gai3} (G α_{13} -Whirlin-Myo15^{CTD}-Eps8^{NTD}), and 5xTCD condensates. We found that addition of Gpsm2 (but not G α_{13}) to the 3xTCD significantly increased the number of liquid-like droplets (Fig. 5C). Further addition of G α_{13} into the resulting 4xTCD^{Gpsm2} did not further increase the number (Fig. 5C). In addition, we also compared the threshold concentration for LLPS among different complexes. As we demonstrated previously (14), Eps8^{NTD} alone and Eps8^{NTD}-Myo15^{CTD} complex did not form LLPS even at their individual concentration of 30 μM . The 3xTCD formed LLPS at their individual concentration of 5 μM , while 4xTCD^{Gpsm2} (but not 4xTCD^{Gai3}) and 5xTCD formed LLPS at much lower threshold concentration of \sim 1 μM (Fig. 5D). These data suggested that Gpsm2, but not Gai, enhanced LLPS of 3xTCD. The promotion effect is most likely due to the phase separation of Gpsm2, as mutations of Gpsm2 (i.e., Gpsm2^{KA} and Gpsm2^{R318RfsX8}) that impaired the LLPS of Gpsm2 also showed defects in assembly of 5xTCD condensates (Fig. 5, C and D). Consistently, Gai did not form LLPS by its own (fig. S7). It should be noted that the threshold concentration for 5xTCD was close to or

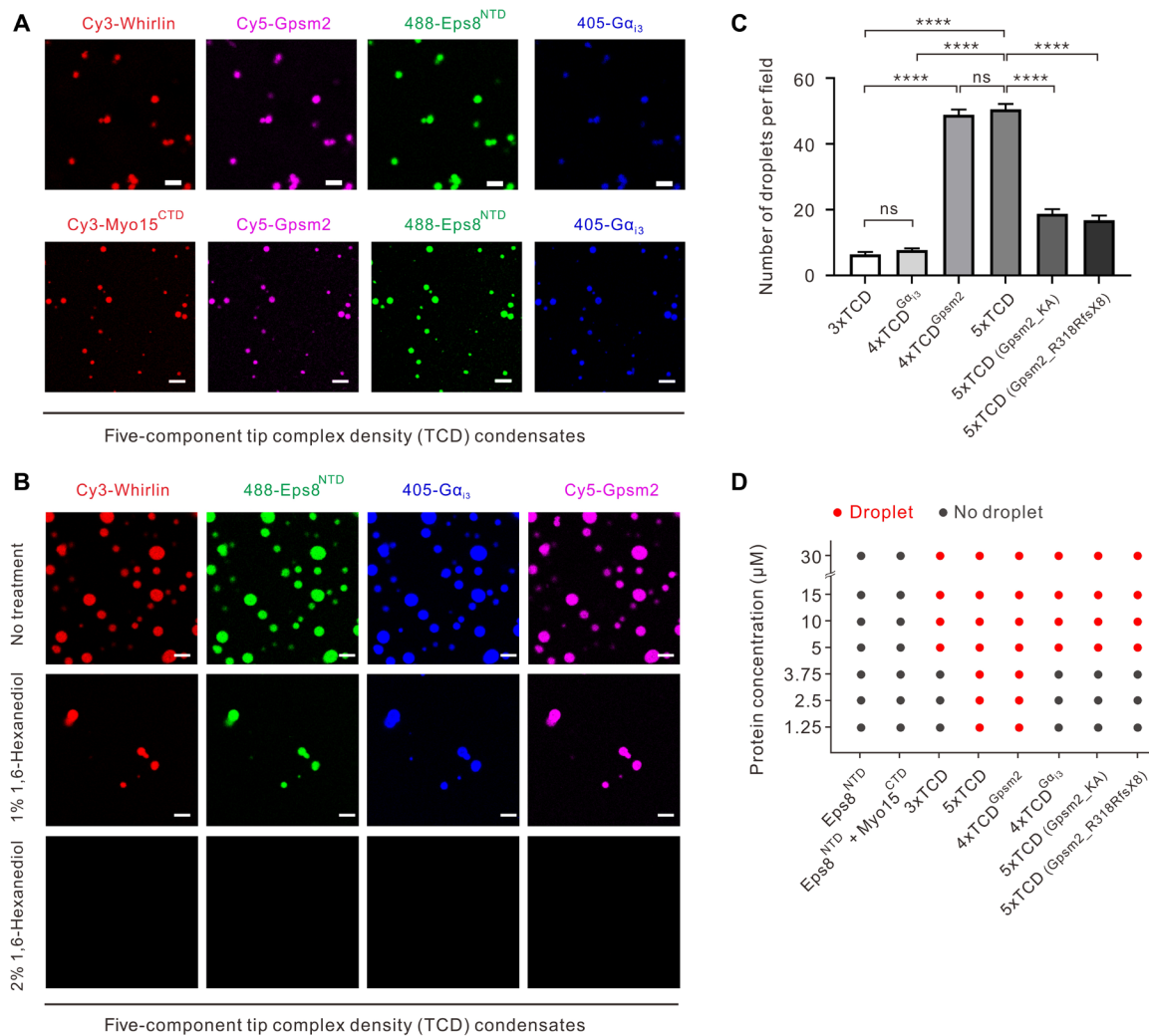


Fig. 5. Gpsm2-Gai significantly promotes formation of the five-component tip complex condensates. (A) Representative fluorescence images showing that mixture of Whirlin, Myo15^{CTD}, Eps8^{NTD}, Gpsm2, and G α_{13} at their individual concentration of 5 μ M led to formation of the liquid-like codroplets. Top: Whirlin, Eps8^{NTD}, Gpsm2, and G α_{13} were labeled with Cy3, Alexa Fluor 488, Cy5, and Alexa Fluor 405, respectively, with each at 1% level. Bottom: Myo15^{CTD}, Eps8^{NTD}, Gpsm2, and G α_{13} were labeled with Cy3, Alexa488, Cy5, and Alexa405, respectively, with each at 1% level. Scale bar, 5 μ m. (B) Treatment of 1,6-hexanediol greatly impaired the LLPS of the 5xTCD condensates. Scale bar, 5 μ m. The concentration of each component was 15 μ M. (C) Quantification data of the number of the liquid-like droplets formed by 3xTCD (Whirlin-Myo15^{CTD}-Eps8^{NTD}), 4xTCD^{Gpsm2} (Gpsm2-Whirlin-Myo15^{CTD}-Eps8^{NTD}), 4xTCD^{Gai3} (G α_{13} -Whirlin-Myo15^{CTD}-Eps8^{NTD}), wild-type 5xTCD condensates, and 5xTCD with Gpsm2 mutations (i.e., Gpsm2^{KA} mutant and Gpsm2^{R318RfsX8} mutant). Data were presented as means \pm SEM from three independent experiments (six fields for each experiment) using Student's *t* test (*****P* < 0.0001; ns, not significant). (D) Phase separation diagram of different tip complex components at indicated concentrations. Highlighted red dots, phase separation; gray dots: no phase separation.

even lower than 1 μ M, suggesting that the 5xTCD condensates may form at the physiological conditions.

5xTCD condensates induce robust actin bundling

How can the 5xTCD condensates contribute to additional actin elongation at the tallest stereocilia? We next wanted to investigate the correlation between the TCD condensates and actin cytoskeleton dynamics. To this end, we carried out the actin-bundling experiments in the presence of various TCD condensates (Fig. 6A). We used Eps8^{FL} here because Eps8^{CTD} is necessary for actin bundling (Fig. 1B) (33). Therefore, Eps8 used in the following actin bundling experiments was its full-length form. As expected, Eps8^{FL} alone could induce actin bundling, although with sporadic actin bundles (Fig. 6A).

Addition of Myo15^{CTD} to Eps8^{FL} did not change the activity much (Fig. 6, A and B). The 3xTCD condensates significantly produced more bundled actin filaments, as described in our previous work (14). Consistent with their phase separation abilities (Fig. 5, C and D), 4xTCD^{Gpsm2} condensates exhibited much stronger actin-bundling ability than 3xTCD condensates did, while 5xTCD condensates displayed similar ability as 4xTCD^{Gpsm2} condensates did (Fig. 6, A and B).

Moreover, we used transmission electron microscopy (TEM) to directly visualize actin bundles in the presence of the tip complex condensates. In line with the observation in fluorescent microscopy assays, thicker actin bundles were observed under TEM when 5xTCD or 4xTCD^{Gpsm2} condensates were added in the system than those in 3xTCD condensates (Fig. 6, C and D). The five-component complex

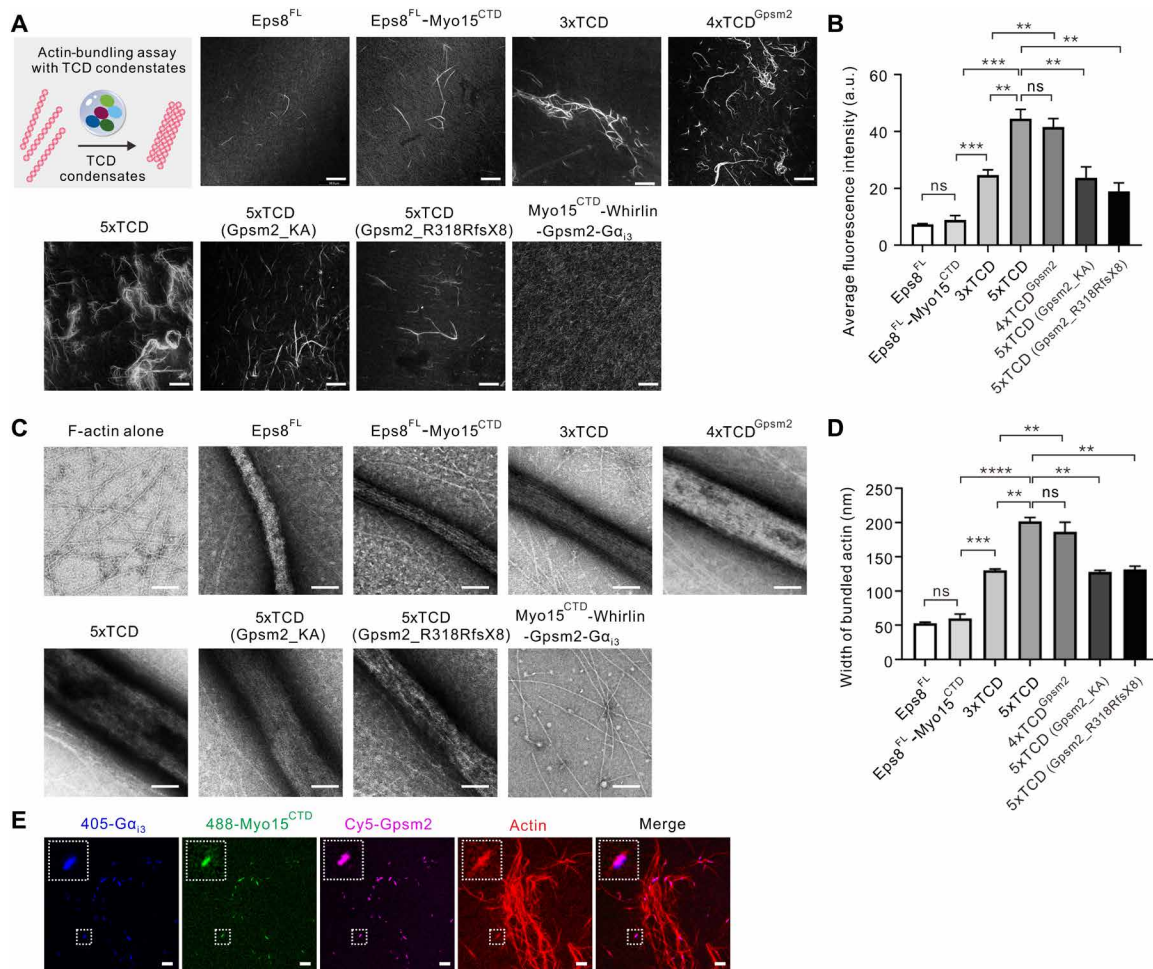


Fig. 6. The five-component tip complex condensates induce much stronger actin bundling than those without Gpsm2-Gai. (A) Representative images under fluorescent microscopy showing that wild-type five-component tip complex condensates have the strongest actin-bundling ability. Scale bar, 25 μm . A diagram showing the process of actin-bundling experiment in vitro is also indicated. (B) Quantitative analysis of the average fluorescence intensities of actin bundles in (A). Average fluorescence intensity was calculated by dividing the total fluorescence intensity (subtracting out background signal) by the total area of a given field. Note that the size of the selected fields in this statistical process was the same. Statistics were performed by two-tailed Student's *t* test. Results were represented as means \pm SEM from six fields ($n = 6$). $***P < 0.001$, $**P < 0.01$. a.u., arbitrary units. (C) Representative images of actin bundles induced by various wild-type and mutant forms of the tip complex mixture under TEM. Scale bar, 100 nm. (D) Distribution of the width of actin bundles from the different groups of experiments. Statistics were performed by two-tailed Student's *t* test. All data were represented as means \pm SEM from six fields ($n = 6$). $****P < 0.0001$, $***P < 0.001$, and $**P < 0.01$. (E) The five-component droplets colocalized with F-actin bundles. Rhodamine-phalloidin was used to label F-actin. Scale bar, 5 μm .

formed codroplets at their individual concentration corresponding to those in the actin-bundling assay (fig. S8). The 5xTCD components colocalized into small consecutive puncta along with F-actin bundles (Fig. 6E), suggesting that the 5xTCD condensates may act along the F-actin bundles. To further prove that the robust actin-bundling activity of the 5xTCD condensates was attributed to LLPS, we took advantage of the Gpsm2^{KA} mutant characterized in Fig. 3 because this mutant is expected not to affect any of the interactions among the five-component complex, but instead, it significantly impaired LLPS of the 5xTCD condensates (Figs. 5C and 3F). Satisfyingly, the tip complex mixture with the Gpsm2^{KA} mutant showed limited actin-bundling capability compared with its wild-type counterpart (Fig. 6, A to D). As expected, the tip complex with the CMCS-associated mutation of Gpsm2, Gpsm2^{R318RfsX8}, showed reduced actin bundles as well (Fig. 6, A to D), probably due to its weakened

LLPS ability. These data suggested that formation of the 5xTCD condensates via LLPS is crucial for robust actin-bundling activity at the tips of the tallest stereocilia and consequently may define hair bundle row identity.

DISCUSSION

Staircase-like architecture of hair cell stereocilia is crucial for auditory perception, but little is known about how this planar asymmetry is achieved. Recently, several elegant studies on planar cell polarity may provide important clues. In the development of stereocilia, planar-polarized enrichment of Gpsm2-Gai at a microvilli-free compartment in the apical surface of hair cells enables their specific localization at row 1 immediately adjacent to the microvilli exclusion zone. At the tips of the tallest stereocilia, Gpsm2-Gai interacts

with the Whirlin-Myo15-Eps8 complex to build a five-component tip complex. It is believed that the complex greatly elongates row 1 and specifies the tallest stereocilia. Given that Gpsm2-Gai complex does not directly involve in actin dynamics, it is still puzzling how Gpsm2-Gai defines the hair bundle row identity.

An interesting observation of our present study may offer critical insights. We find that Gpsm2 can autonomously form LLPS in vitro and in cells. Moreover, the row 1-specific five-component tip complex could also form LLPS. The 5xTCD condensates display much stronger phase separation ability and actin-bundling capability than those without Gpsm2-Gai (Figs. 5 and 6). The promotion effect is mainly attributed to the LLPS of Gpsm2, as a mutant of Gpsm2 (Gpsm2^{KA}) that interferes with its LLPS largely impairs the 5xTCD condensates formation and actin bundling (Figs. 5 and 6). Notably, the fact that Gpsm2-Gai-Whirlin-Myo15^{CTD} complex (5xTCD without Eps8) did not induce actin bundling at all demonstrates that Eps8 was the only actin-bundling factor among the complex (Fig. 6).

How does the robust actin bundling event contribute to the over-elongation of the tallest stereocilia? Such an actin bundle-lengthening property of Eps8 may stem from the ability of actin bundling to stabilize the actin core of stereocilia that further facilitates the actin polymerization at the dynamic filament ends in the tallest stereocilia (34). Alternatively, Eps8-induced actin bundling may cause pronounced barbed-end elongation and thereby makes a longer bundle, as Espin (another actin-bundling protein) does in microvilli (35). It should be noted that the 5xTCD condensates might enhance actin polymerization/nucleation in addition to actin bundling, possibly by condensing higher amounts of Myo15 at row 1, especially when the motor domain of Myo15 was shown to directly accelerate actin filament polymerization by driving nucleation (36). Unfortunately, because of the technical challenges, we were unable to obtain qualified full-length Myo15 protein to prove this point in the current work. However, our reconstitution experiment has demonstrated that the row 1-specific condensates can condense Myo15^{CTD}; hence, it is reasonable to believe that full-length Myo15 would be enriched at row 1 to facilitate hair bundle elongation. Therefore, we propose that Gpsm2-Gai significantly promotes formation of LLPS-mediated 5xTCD condensates that, in turn, largely enrich Eps8 and Myo15 to induce robust actin elongation at the tips of the tallest stereocilia (Fig. 7). Consistently, a recent study has showed that, in *Gpsm2*^{-/-} mutant hair cells, stereocilia are uniformly short, and Myo15-Eps8 is distributed in comparable amounts among all rows, which is in sharp contrast with that in wild-type mice where Myo15-Eps8 is predominantly localized at the tips of the tallest stereocilia (most likely via enrichment effect of row 1-specific TCD condensates) (21).

Compared with Gpsm2, Gai seems to be dispensable for promotion of LLPS. This is expected because Gai could not form LLPS by its own (fig. S7) and therefore would not add valency into the system to further promote LLPS. We believe that cortical localized Gai may serve as an adaptor between the 5xTCD condensates and cortical membrane, thus acting as a cortical anchoring site for the actin elongation machinery (including but not limited to the 5xTCD condensates). Therefore, it would not be unexpected that depletion of Gai would lead to defects of stereocilia elongation and first row identity as reported previously because the actin elongation machinery would lose its cortical anchoring site in the absence of Gai. This is reminiscent of the scenario in asymmetric cell division where Gai functions as a linker between apical cortical membrane and spindle orientation machinery such as Gpsm2-NuMA complex (28).

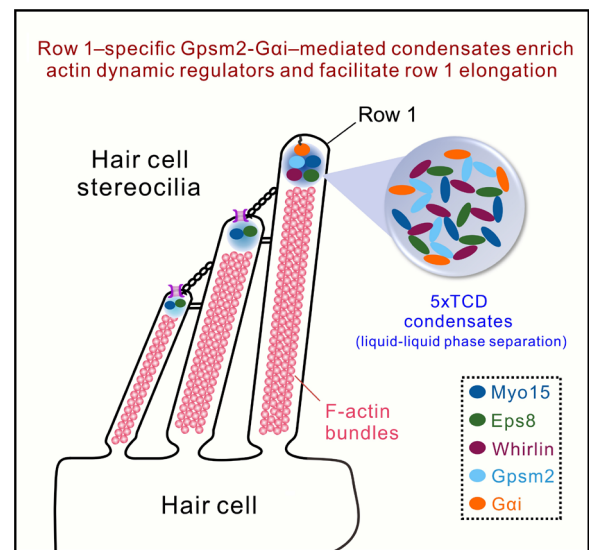


Fig. 7. A model depicting that row 1-specific Gpsm2-Gai-mediated condensates enrich actin dynamic regulators and facilitate row 1 elongation. In the developing stereocilia, Gpsm2-Gai is restrictedly transported to the tips of the tallest stereocilia where they form a five-component complex with Whirlin-Myo15-Eps8. Gpsm2-Gai notably promotes the 5xTCD condensates that, in turn, effectively enrich actin dynamic regulators (including but not limited to Eps8 and Myo15) and facilitate robust actin elongation at the tips of the tallest stereocilia. In contrast, shorter rows are unable to generate stereocilia with a comparable height, most likely because of lack of Gpsm2-Gai that leads to weakened phase separation ability and actin elongation capability.

Loss of Gai resulted in severe defective asymmetric cell divisions due to the mislocalization of the spindle orientation machinery during the process (37, 38).

How is the assembly/disassembly of the row 1-specific TCD condensates regulated? How are these regulatory processes correlated with stereocilia development? We believe that at least two issues should be taken into account: (i) timing of the interactions among the tip complex and (ii) protein level of the tip complex. Our data show that the protein concentration is critical for LLPS formation. The threshold concentration that promotes Gpsm2 LLPS is about 10 μM ; the five-component tip complex could undergo LLPS at their individual concentration of $\sim 1 \mu\text{M}$. It should be mentioned that we used a truncation form of Myo15 in the current study. Full-length Myo15 may work as a dimer, which would further expand the valency of the system and lower the threshold concentration of LLPS. In the developing stereocilia, Myo15 and Eps8 formed an early tip complex already broadly enriched at E16.5 (21). By contrast, Whirlin, Gpsm2, and Gai were highly enriched at the exclusion zone at E16.5, and they were enriched at tips at later stages to form the five-component tip complex specific to row 1 (21). When the concentration of tip-accumulated five components reaches the threshold concentration of LLPS, the 5xTCD condensates form autonomously and trigger robust actin elongation event. In support of this idea, Krey *et al.* (39) recently found that the protein level of the TCD components were temporally regulated during development. Notably, enrichment of the above proteins at tips of the tallest stereocilia was highly correlated with the elongation of row 1 (39). At the mature stage (P21.5), the protein level sharply decreased (39), probably because of gene transcription and/or expression regulation

or protein degradation system. It is most likely that accumulation of row 1-specific tip complex leads to formation of TCD condensates that promotes robust actin elongation event, while reduction of protein level disrupts LLPS and subsequently stops the elongation process.

We understand that direct investigation of the TCD condensates in hair cells is still challenging at current stage because of technical limit, and future work is definitely needed to demonstrate their critical roles in stereocilia development. Nevertheless, our work provides a proof of concept that condensation of row 1-specific tip complex via LLPS may underlie hair bundle row identity.

MATERIALS AND METHODS

Protein expression and purification

The coding sequences of Whirlin (GenBank: AB040959.1), Gpsm2 (GenBank: NM_029522.2), AGS3 (GenBank: NM_001355574.1), $\text{G}\alpha_{13}$ (GenBank: NM_006496.3), Myo15 (GenBank: NM_010862.2), and Eps8 (GenBank: NM_007945.3) were cloned into a previously described modified pET32a vector with a Trx tag and a His₆-tag at its N terminus (14). Primers of all constructs are listed in table S2. For the GST pull-down assays, various fragments of Whirlin were cloned into the pGEX-4T-1 vector. Mutations were created through site-directed mutagenesis method and confirmed by DNA sequencing. All constructs were expressed in *Escherichia coli* BL21 (DE3) (Transgen Biotech; catalog no. CD601) or Codon Plus (WeidiBio; catalog no. EC1007) host cells at 16°C for 18 hours induced by 0.2 mM isopropyl- β -D-thiogalactoside (final concentration). Recombinant proteins were purified as previously described (14). In general, His₆-tagged and GST-tagged proteins were purified by Ni²⁺-nitrilotriacetic acid agarose affinity chromatography and GSH [glutathione (reduced form)]-sepharose affinity chromatography, respectively. Eluted target proteins were further purified by a size exclusion chromatography (SEC) (HiLoad 26/600 Superdex 200 pg, Cytiva) in the buffer of 50 mM tris (pH 8.0), 300 mM NaCl, 1 mM dithiothreitol (DTT), and 1 mM EDTA. For the reconstitution of the tip complex, His-tagged proteins were cleaved by human rhinovirus 3C protease at 4°C overnight and then purified by another step of SEC purification.

ITC assay

ITC assays were performed on a MicroCal iTC200 system (Malvern Panalytical, UK) at 25°C. Various Gpsm2^{TPR} and Whirlin^{GBD} fragments were dissolved in the buffer containing 50 mM tris (pH 8.0), 100 mM NaCl, 1 mM EDTA, and 1 mM DTT. The Whirlin^{GBD} proteins (~500 μ M) were loaded into syringe, and the Gpsm2^{TPR} proteins (~50 μ M) were loaded into the cell. In each titration, 2- μ l aliquot of protein in the syringe was injected into the cell, and the time interval was 120 s to make sure that the titration peak returned to the baseline. Titration data were fitted with the one-site binding model using Origin 7.0.

GST pull-down assay

Freshly purified His₆-Gpsm2^{TPR} was incubated with various forms of GST-Whirlin fragments for 1 hour at 4°C. After centrifugation for 10 min at 4°C, the supernatant was loaded into 30- μ l GSH-sepharose 4B slurry beads to incubate for 30 min at 4°C. After washing with PBS buffer three times, the bound proteins were eluted by boiling with 30 μ l of 2 \times SDS-polyacrylamide gel electrophoresis loading dye and detected by Western blot using anti-His antibody (Smart-lifesciences, catalog no. SLAB28; 1:5000).

Crystallization, data collection, and structure determination

To obtain stable Gpsm2^{TPR}-Whirlin^{GBD} complex, Gpsm2^{TPR} (amino acids 15 to 350) was fused with Whirlin^{GBD} (amino acids 717 to 746). The best crystals of the fusion protein (~10 mg/ml) were obtained by the hanging drop diffusion method at 16°C in the buffer containing 1.2 M ammonium tartrate dibasic and 0.1 M tris (pH 8.8). Crystals were cryoprotected in the corresponding reservoir solution with 25% glycerol before x-ray diffraction experiments. The diffraction data were collected at BL41XU at Spring-8 (Hyogo, Japan). The diffraction data were processed with XDS (40). The complex structure was solved by the molecular replacement method using the structure of Gpsm2^{TPR} in Gpsm2-NuMA complex (Protein Data Bank code: 3RO2) as the searching model through the software suits of Phaser (41). Further refinement was performed using Phenix (42) and Coot (43). The final refinement statistics of the complex structures are listed in table S1. Structural diagrams were prepared by PyMOL.

Protein labeling with fluorophore

Freshly purified untagged proteins were labeled as described previously (14). In general, proteins were first dissolved in the buffer containing 300 mM NaCl, 100 mM NaHCO₃ (pH 8.3), and 4 mM β -mercaptoethanol (β -ME). Cy-3/Cy5 N-hydroxysuccinimide (NHS) ester (AAT Bioquest; catalog no. 271/280) and Alexa Fluor 405/488 NHS ester (Thermo Fisher Scientific; catalog no. A30000/A20000) were dissolved in dimethyl sulfoxide and incubated with the indicated proteins (molar ratio of 1:1) at room temperature for 1 hour. The labeling reaction was quenched by addition of the buffer of 200 mM tris (pH 8.2). The mixture was then purified with a HiTrap desalting column with the buffer containing 50 mM tris (pH 8.0), 300 mM NaCl, and 4 mM β -ME to remove the unlabeled fluorophore. Fluorescence labeling efficiency was determined by NanoDrop 2000 (Thermo Fisher Scientific).

In vitro phase separation assay

All freshly purified and labeled proteins were dissolved in the buffer containing 50 mM tris (pH 8.0), 300 mM NaCl, and 4 mM β -ME. After centrifugation at 16,873g for 10 min at 4°C, samples were placed on ice before the phase separation assay. Each phase separation sample was made by mixing of indicated labeled proteins at indicated concentrations for 10 min at 25°C. Each sample was then injected into a homemade chamber as described previously (44) for fluorescence imaging (Leica TCS SP8).

FRAP assay

FRAP assay was performed as previously described (14). In brief, the assay was carried out on a Leica SP8 confocal microscope. For Cy3-labeled protein droplets, a circular region of interest (ROI) was bleached by a 561-nm laser beam at room temperature. For FRAP assay on liquid-phase droplets in living cell, HEK293T cells (American Type Culture Collection; catalog no. CRL-3216; Research Resource Identifiers: CVCL_0063) were cultured on glass-bottom dishes (MatTek) and transfected with the indicated plasmids. GFP and RFP signals were bleached with 488- and 561-nm laser beams at 37°C, respectively. For each experiment, the fluorescence intensity of a neighboring droplet with similar size to the bleached one was also recorded for intensity correction. Background intensity was subtracted before data analysis. The ROI intensity at time 0 s (right after the photobleaching) was set as 0%, and the prebleaching intensity was normalized to 100%.

Actin-bundling assay

To obtain preassembled F-actin filament, monomeric rabbit G-actin (Cytoskeleton) was induced to polymerize for 1 hour at room temperature in the polymerization buffer containing 50 mM tris (pH 8.0), 1 mM adenosine 5'-triphosphate, 0.5 mM DTT, 0.2 mM CaCl₂, 2 mM MgCl₂, and 50 mM KCl. Freshly purified wild-type and mutant form of five-component tip complex mixture and other tip complexes without Gpsm2-Gα_{i3} were incubated with the above preassembled F-actin (~2 μM) at room temperature for 1 hour. Actin was then labeled with rhodamine-phalloidine (Cytoskeleton) for 15 min. The samples were carefully mounted between a slide and a coverslip and imaged by fluorescence microscopy (Leica TCS SP8). In these assays, the concentration of each component was shown as follows: Eps8^{FL}, 0.25 μM; Whirlin, 0.5 μM; Myo15^{CTD}, 0.5 μM; Gpsm2 WT/mutants, 0.5 μM; Gα_{i3}, 0.5 μM; F-actin, ~2 μM.

Samples for TEM (Tecnai G2 Spirit 120 kV) were adsorbed to glow-discharged, carbon-coated formvar films on copper grids for 1 min and negatively stained with 0.75% (m/v) uranium acetate for 45 s. The concentration of each component in this assay was shown as follows: Eps8^{FL}, 0.25 μM; Whirlin, 1 μM; Myo15^{CTD}, 1 μM; Gpsm2 wild type/mutants, 1 μM; Gα_{i3}, 1 μM; F-actin, ~2 μM.

Statistical analyses

All statistics [e.g., number of samples (*n*) and biological replicates (*N*) for all experiments] were described in the figure legends. All data were represented as means ± SEM using the two-tailed Student's *t* test, using GraphPad Prism. All experiments were performed at least three times independently.

SUPPLEMENTARY MATERIALS

Supplementary material for this article is available at <https://science.org/doi/10.1126/sciadv.abn4556>

[View/request a protocol for this paper from Bio-protocol.](#)

REFERENCES AND NOTES

- P. G. Gillespie, U. Muller, Mechanotransduction by hair cells: Models, molecules, and mechanisms. *Cell* **139**, 33–44 (2009).
- P. G. Barr-Gillespie, Assembly of hair bundles, an amazing problem for cell biology. *Mol. Biol. Cell* **26**, 2727–2732 (2015).
- B. Kachar, M. Parakkal, M. Kurc, Y. Zhao, P. G. Gillespie, High-resolution structure of hair-cell tip links. *Proc. Natl. Acad. Sci. U.S.A.* **97**, 13336–13341 (2000).
- G. P. Richardson, C. Petit, Hair-bundle links: Genetics as the gateway to function. *Cold Spring Harb. Perspect. Med.* **9**, a033142 (2019).
- D. N. Furness, C. M. Hackney, Cross-links between stereocilia in the guinea pig cochlea. *Hear. Res.* **18**, 177–188 (1985).
- C. L. Cunningham, U. Muller, Molecular structure of the hair cell mechano-electrical transduction complex. *Cold Spring Harb. Perspect. Med.* **9**, (2019).
- A. K. Rzadzinska, M. E. Schneider, C. Davies, G. P. Riordan, B. Kachar, An actin molecular treadmill and myosins maintain stereocilia functional architecture and self-renewal. *J. Cell Biol.* **164**, 887–897 (2004).
- M. M. Mogensen, A. Rzadzinska, K. P. Steel, The deaf mouse mutant whirler suggests a role for whirlin in actin filament dynamics and stereocilia development. *Cell Motil. Cytoskeleton* **64**, 496–508 (2007).
- I. A. Belyantseva, E. T. Boger, S. Naz, G. I. Frolenkov, J. R. Sellers, Z. M. Ahmed, A. J. Griffith, T. B. Friedman, Myosin-XVa is required for tip localization of whirlin and differential elongation of hair-cell stereocilia. *Nat. Cell Biol.* **7**, 148–156 (2005).
- V. Zampini, L. Ruttiger, S. L. Johnson, C. Franz, D. N. Furness, J. Waldhaus, H. Xiong, C. M. Hackney, M. C. Holley, N. Offenhauser, P. P. Di Fiore, M. Knipper, S. Masetto, W. Marcotti, Eps8 regulates hair bundle length and functional maturation of mammalian auditory hair cells. *PLoS Biol.* **9**, e1001048 (2011).
- H. W. Lin, M. E. Schneider, B. Kachar, When size matters: the dynamic regulation of stereocilia lengths. *Curr. Opin. Cell Biol.* **17**, 55–61 (2005).
- F. J. Probst, R. A. Fridell, Y. Raphael, T. L. Saunders, A. Wang, Y. Liang, R. J. Morell, J. W. Touchman, R. H. Lyons, K. Noben-Trauth, T. B. Friedman, S. A. Camper, Correction of deafness in shaker-2 mice by an unconventional myosin in a BAC transgene. *Science* **280**, 1444–1447 (1998).
- P. Mburu, M. Mustapha, A. Varela, D. Weil, A. El-Amrouri, R. H. Holme, A. Rump, R. E. Hardisty, S. Blanchard, R. S. Coimbra, I. Perfettini, N. Parkinson, A. M. Mallon, P. Glenister, M. J. Rogers, A. J. Paige, L. Moir, J. Clay, A. Rosenthal, X. Z. Liu, G. Blanco, K. P. Steel, C. Petit, S. D. Brown, Defects in whirlin, a PDZ domain molecule involved in stereocilia elongation, cause deafness in the whirler mouse and families with DFNB31. *Nat. Genet.* **34**, 421–428 (2003).
- L. Lin, Y. Shi, M. Wang, C. Wang, Q. Lu, J. Zhu, R. Zhang, Phase separation-mediated condensation of Whirlin-Myo15-Eps8 stereocilia tip complex. *Cell Rep.* **34**, 108770 (2021).
- U. Manor, A. Dianza, M. Grati, L. Andrade, H. Lin, P. P. Di Fiore, G. Scita, B. Kachar, Regulation of stereocilia length by myosin XVa and whirlin depends on the actin-regulatory protein Eps8. *Curr. Biol.* **21**, 167–172 (2011).
- B. Tarchini, C. Jolicoeur, M. Cayouette, A molecular blueprint at the apical surface establishes planar asymmetry in cochlear hair cells. *Dev. Cell* **27**, 88–102 (2013).
- J. Ezan, L. Lasvaux, A. Gezer, A. Novakovic, H. May-Simera, E. Belotti, A. C. Lhoumeau, L. Birnbaumer, S. Beer-Hammer, J. P. Borg, A. Le Bivic, B. Nurnberg, N. Sans, M. Montcouquiol, Primary cilium migration depends on G-protein signalling control of subapical cytoskeleton. *Nat. Cell Biol.* **15**, 1107–1115 (2013).
- B. Tarchini, A. L. Tadenev, N. Devanney, M. Cayouette, A link between planar polarity and staircase-like bundle architecture in hair cells. *Development* **143**, 3926–3932 (2016).
- J. Ezan, M. Montcouquiol, Revisiting planar cell polarity in the inner ear. *Semin. Cell Dev. Biol.* **24**, 499–506 (2013).
- P. Jean, O. D. Ozcete, B. Tarchini, T. Moser, Intrinsic planar polarity mechanisms influence the position-dependent regulation of synapse properties in inner hair cells. *Proc. Natl. Acad. Sci. U.S.A.* **116**, 9084–9093 (2019).
- A. L. D. Tadenev, A. Akturk, N. Devanney, P. D. Mathur, A. M. Clark, J. Yang, B. Tarchini, GPSM2-GNAI specifies the tallest stereocilia and defines hair bundle row identity. *Curr. Biol.* **29**, 921–934.e4 (2019).
- Y. Bhonker, A. Abu-Rayyan, K. Ushakov, L. Amir-Zilberstein, S. Shivatzki, O. Yizhar-Barnea, T. Elkan-Miller, E. Tayeb-Fligelman, S. M. Kim, M. Landau, M. Kanaan, P. Chen, F. Matsuzaki, D. Sprinzak, K. B. Avraham, The GPSM2/LGN GoLoco motifs are essential for hearing. *Mamm. Genome* **27**, 29–46 (2016).
- S. A. Mauriac, Y. E. Hien, J. E. Bird, S. D. Carvalho, R. Peyrourou, S. C. Lee, M. M. Moreau, J. M. Blanc, A. Geysler, C. Medina, O. Thoumine, S. Beer-Hammer, T. B. Friedman, L. Ruttiger, A. Forge, B. Nurnberg, N. Sans, M. Montcouquiol, Defective Gpsm2/Gα_{i3} signalling disrupts stereocilia development and growth cone actin dynamics in Chudley-McCullough syndrome. *Nat. Commun.* **8**, 14907 (2017).
- S. Beer-Hammer, S. C. Lee, S. A. Mauriac, V. Leiss, I. A. M. Groh, A. Novakovic, R. P. Piekorz, K. Bucher, C. Chen, K. Ni, W. Singer, C. Harasztsosi, T. Schimmang, U. Zimmermann, K. Pfeiffer, L. Birnbaumer, A. Forge, M. Montcouquiol, M. Knipper, B. Nurnberg, L. Ruttiger, Gai proteins are indispensable for hearing. *Cell. Physiol. Biochem.* **47**, 1509–1532 (2018).
- D. Doherty, A. E. Chudley, G. Coghlan, G. E. Ishak, A. M. Innes, E. G. Lemire, R. C. Rogers, A. A. Mhanni, I. G. Phelps, S. J. Jones, S. H. Zhan, A. P. Fejes, H. Shahin, M. Kanaan, H. Akay, M. Tekin, F. C. Consortium, B. Triggs-Raine, T. Zelinski, GPSM2 mutations cause the brain malformations and hearing loss in Chudley-McCullough syndrome. *Am. J. Hum. Genet.* **90**, 1088–1093 (2012).
- T. Walsh, H. Shahin, T. Elkan-Miller, M. K. Lee, A. M. Thornton, W. Roeb, A. Abu Rayyan, S. Loulus, K. B. Avraham, M. C. King, M. Kanaan, Whole exome sequencing and homozygosity mapping identify mutation in the cell polarity protein GPSM2 as the cause of nonsyndromic hearing loss DFNB82. *Am. J. Hum. Genet.* **87**, 90–94 (2010).
- K. O. Yariz, T. Walsh, H. Akay, D. Duman, A. C. Akkaynak, M. C. King, M. Tekin, A truncating mutation in GPSM2 is associated with recessive non-syndromic hearing loss. *Clin. Genet.* **81**, 289–293 (2012).
- Q. Du, I. G. Macara, Mammalian Pins is a conformational switch that links NuMA to heterotrimeric G proteins. *Cell* **119**, 503–516 (2004).
- M. Carminati, S. Gallini, L. Pirovano, A. Alfieri, S. Bisi, M. Mapelli, Concomitant binding of Afadin to LGN and F-actin directs planar spindle orientation. *Nat. Struct. Mol. Biol.* **23**, 155–163 (2016).
- S. Yuzawa, S. Kamakura, Y. Iwakiri, J. Hayase, H. Sumimoto, Structural basis for interaction between the conserved cell polarity proteins Inscuteable and Leu-Gly-Asn repeat-enriched protein (LGN). *Proc. Natl. Acad. Sci. U.S.A.* **108**, 19210–19215 (2011).
- J. Zhu, W. Wen, Z. Zheng, Y. Shang, Z. Wei, Z. Xiao, Z. Pan, Q. Du, W. Wang, M. Zhang, LGN/mlnsc and LGN/NuMA complex structures suggest distinct functions in asymmetric cell division for the Par3/mlnsc/LGN and Gai/LGN/NuMA pathways. *Mol. Cell* **43**, 418–431 (2011).
- S. Culurgioni, A. Alfieri, V. Pendolino, F. Laddomada, M. Mapelli, Inscuteable and NuMA proteins bind competitively to Leu-Gly-Asn repeat-enriched protein (LGN) during asymmetric cell divisions. *Proc. Natl. Acad. Sci. U.S.A.* **108**, 20998–21003 (2011).

33. A. Disanza, M. F. Carlier, T. E. Stradal, D. Didry, E. Frittoli, S. Confalonieri, A. Croce, J. Wehland, P. P. Di Fiore, G. Scita, Eps8 controls actin-based motility by capping the barbed ends of actin filaments. *Nat. Cell Biol.* **6**, 1180–1188 (2004).
34. A. Rzadzinska, M. Schneider, K. Noben-Trauth, J. R. Bartles, B. Kachar, Balanced levels of Espin are critical for stereocilia growth and length maintenance. *Cell Motil. Cytoskeleton* **62**, 157–165 (2005).
35. P. A. Loomis, L. Zheng, G. Sekerkova, B. Changyaleket, E. Mugnaini, J. R. Bartles, Espin cross-links cause the elongation of microvillus-type parallel actin bundles in vivo. *J. Cell Biol.* **163**, 1045–1055 (2003).
36. Z. G. Moreland, F. Jiang, C. Aguilar, M. Barzik, R. Gong, A. Shams, C. Faaborg-Andersen, J. C. Werth, R. Harley, D. C. Sutton, S. M. Cole, A. Parker, S. Morse, E. Wilson, Y. Takagi, J. R. Sellers, S. D.M. Brown, T. B. Friedman, G. M. Alushin, M. R. Bowl, J. E. Bird, Myosin-driven nucleation of actin filaments drives stereocilia development critical for hearing. *bioRxiv* 2021.07.09.451618 [Preprint] 13 July 2021. <https://doi.org/10.1101/2021.07.09.451618>.
37. F. S. Willard, Z. Zheng, J. Guo, G. J. Digby, A. J. Kimple, J. M. Conley, C. A. Johnston, D. Bosch, M. D. Willard, V. J. Watts, N. A. Lambert, S. R. Ikeda, Q. Du, D. P. Siderovski, A point mutation to $G\alpha_i$ selectively blocks GoLoco motif binding: Direct evidence for $G\alpha$ -GoLoco complexes in mitotic spindle dynamics. *J. Biol. Chem.* **283**, 36698–36710 (2008).
38. E. Peyre, F. Jaouen, M. Saadaoui, L. Haren, A. Merdes, P. Durbec, X. Morin, A lateral belt of cortical LGN and NuMA guides mitotic spindle movements and planar division in neuroepithelial cells. *J. Cell Biol.* **193**, 141–154 (2011).
39. J. F. Krey, P. Chatterjee, R. A. Dumont, M. O'Sullivan, D. Choi, J. E. Bird, P. G. Barr-Gillespie, Mechanotransduction-dependent control of stereocilia dimensions and row identity in inner hair cells. *Curr. Biol.* **30**, 442–454.e7 (2020).
40. W. Kabsch, XDS. *Acta Crystallogr. D Biol. Crystallogr.* **66**, 125–132 (2010).
41. A. J. McCoy, R. W. Grosse-Kunstleve, P. D. Adams, M. D. Winn, L. C. Storoni, R. J. Read, Phaser crystallographic software. *J. Appl. Cryst.* **40**, 658–674 (2007).
42. P. D. Adams, P. V. Afonine, G. Bunkoczi, V. B. Chen, I. W. Davis, N. Echols, J. J. Headd, L. W. Hung, G. J. Kapral, R. W. Grosse-Kunstleve, A. J. McCoy, N. W. Moriarty, R. Oeffner, R. J. Read, D. C. Richardson, J. S. Richardson, T. C. Terwilliger, P. H. Zwart, PHENIX: a comprehensive Python-based system for macromolecular structure solution. *Acta Crystallogr. D Biol. Crystallogr.* **66**, 213–221 (2010).
43. P. Emsley, K. Cowtan, Coot: model-building tools for molecular graphics. *Acta Crystallogr. D Biol. Crystallogr.* **60**, 2126–2132 (2004).
44. J. Zhu, Q. Zhou, Y. Xia, L. Lin, J. Li, M. Peng, R. Zhang, M. Zhang, GIT/PIX condensates are modular and ideal for distinct compartmentalized cell signaling. *Mol. Cell* **79**, 782–796.e6 (2020).

Acknowledgments: We thank members of the Shanghai Synchrotron Radiation Facility (SSRF, China; beamlines BL02U1, BL18U1, and BL19U1) and Spring-8 (Hyogo, Japan; beamline BL41XU) for x-ray beam time and the staff members of the Large-scale Protein Preparation System, Electron Microscopy System, and Molecular Imaging System at the National Facility for Protein Science in Shanghai (NFPS), Zhangjiang Laboratory, China for providing technical support and assistance in data collection and analysis. **Funding:** This work was supported by grants from the National Key R&D Program of China (2018YFA0507900 to J.Z. and 2019YFA0508402 to C.W.), grants from the National Natural Science Foundation of China (32122036, U2032122, and 31770779 to J.Z.; 22122703, 91953110, and 32170767 to C.W.), a grant from Science and Technology Commission of Shanghai Municipality (20S11900200) and a grant from the Interdisciplinary Innovative Talent Training Program of Shanghai Jiao Tong University to J.Z., a grant from University of Science and Technology of China Research Funds of Double First-Class Initiative (YD9100002006) and a grant from the Fundamental Research Funds for the Central Universities (WK9100000029) to C.W., and a grant from the Scientific Research Foundation for Youth Scholars of Shanghai Jiao Tong University (AF0890029) to L.L. C.W. is supported by the Chinese Academy of Sciences Pioneer Hundred Talents Program. **Author contributions:** J.Z., Y.S., L.L., and C.W. designed the experiments. Y.S. and L.L. performed the biochemical experiments and carried out the x-ray data collection. L.L. determined the crystal structure. All authors analyzed the data. J.Z., Y.S., and L.L. drafted the manuscript. J.Z. coordinated the project. All authors revised the draft and approved the final version of the manuscript. **Competing interests:** The authors declare that they have no competing interests. **Data and materials availability:** All data needed to evaluate the conclusions in the paper are present in the paper and/or the Supplementary Materials. The atomic coordinate of the Gpsm2-Whirlin complex has been deposited to the Protein Data Bank under the accession code: 7EP7.

Submitted 28 November 2021
 Accepted 26 April 2022
 Published 10 June 2022
 10.1126/sciadv.abn4556

Promotion of row 1–specific tip complex condensates by Gpsm2-G*#i* provides insights into row identity of the tallest stereocilia

Yingdong ShiLin LinChao WangJinwei Zhu

Sci. Adv., 8 (23), eabn4556. • DOI: 10.1126/sciadv.abn4556

View the article online

<https://www.science.org/doi/10.1126/sciadv.abn4556>

Permissions

<https://www.science.org/help/reprints-and-permissions>

Use of this article is subject to the [Terms of service](#)